On the Applicability of Source Localization Techniques to Passive Multistatic Radar

Daniel E. Hack*‡, Lee K. Patton*, Braham Himed† and Michael A. Saville†‡
*Matrix Research, Inc., Beavercreek, Ohio 45432; Email: {dan.hack; lee.patton}@matrixresearch.com
†Air Force Research Laboratory, WPAFB, Ohio 45433; Email: {braham.himed; michael.saville}@wpafb.af.mil
‡Dept. of Electrical and Computer Engineering, Air Force Institute of Technology, WPAFB, Ohio 45433

***Abstract*—The source localization problem concerns the detection and localization of an emitter whose transmission is observed by geographically separated receivers. The passive multistatic radar (PMR) problem concerns the detection and localization of a target that scatters an illumination signal to geographically separated receivers. By modeling the scattering target as an emitter, the techniques of source localization can be applied to the PMR problem. Indeed, this approach has recently been introduced in the literature. However, the exact relationship between the two problems has not been made explicit. In this work, we derive a centralized generalized likelihood ratio test (GLRT) detector that performs the processing characteristic of both source localization and PMR. This detector is used to assess the relative detection benefit provided by source localization in PMR. We show that source localization techniques are of limited utility in PMR due to the SNR regimes of the target-scattered and direct-path signals typical of the PMR signal environment.**

I. Introduction

In the source detection and localization problem, the signal emitted by a transmitter is intercepted by multiple, geographically separated receivers, shown in Fig. 1a. The intercepted signals are then jointly processed to detect and localize the emitter. In the passive multistatic radar (PMR) problem, one or multiple illuminators-of-opportunity emit signals that impinge on a target, and the scattered *target-path* signals are intercepted by multiple, geographically separated receivers, shown in Fig. 1b. In addition, the transmitter-to-receiver *direct-path* signals are also intercepted by each receiver. The direct-path and target-path signals are then jointly processed to detect and localize the target. Recognizing that the target in the PMR scenario "emits" the scattered signals enables the application of source detection and localization algorithms to the PMR problem. This paper investigates the application of such techniques to the PMR detection problem.

The conventional approach to PMR detection uses a decentralized architecture, in which detection is performed individually in the bistatic range-Doppler domain for each transmitter-receiver (Tx-Rx) pair, and the resulting detections are combined in a subsequent stage to localize and track targets in Cartesian space [1]. Centralized approaches, in which all measurements are jointly processed to detect and localize targets directly in Cartesian space, have also been investigated [2]. Such approaches are adaptations of techniques used in active multistatic radar to the passive case, in which each Tx-Rx pair localizes the target in bistatic range and bistatic range rate. Geometrically, each Tx-Rx pair constrains the target position to an ellipsoid with foci at the transmitter and receiver locations. We term such processing *Tx-Rx processing*. In contrast, source localization performs pair-wise correlation of the intercepted signals across receivers, termed here *Rx-Rx processing*. Each receiver pair localizes the target in range difference and range difference rate[1]. Geometrically, each Rx-Rx pair constrains the target position to a hyperboloid with foci at the receiver locations.

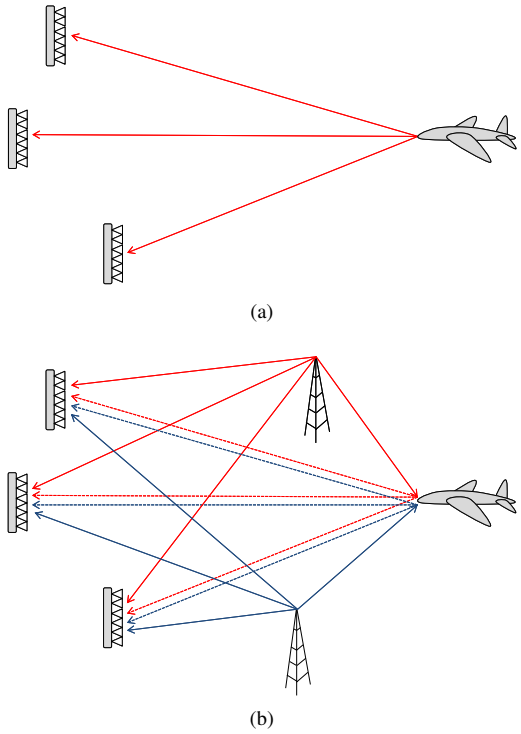

Fig. 1. Depiction of the (a) source localization and (b) passive multistatic radar signal environments.

Recent studies have considered centralized Rx-Rx processing in the PMR context [3], [4], but a full analysis has not yet been provided. In [3], the authors formulate a passive multistatic moving-target imaging procedure that uses Rx-Rx processing only. However, the authors do not account for the direct-path signal, which is the main source of interference

[1]Range difference and range difference rate are often termed time-difference of arrival (TDOA) and frequency difference of arrival (FDOA), respectively.

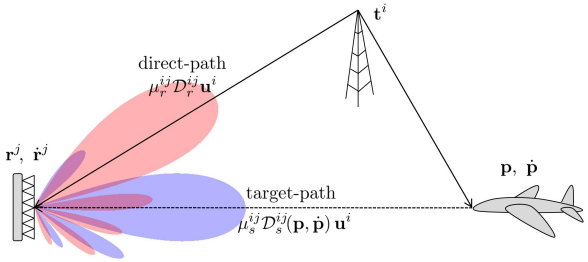

Fig. 2. Geometry and signal environment of the ij^{th} Tx-Rx pair.

in most PMR applications. In addition, the authors assume a coherent target model, which is invalid for complex targets in multistatic scenarios [5]. In [4], the authors present a GLRT statistic based on coherence between appropriately compensated target-path signals. Like [3], their formulation considers only the target-path signal at each receiver. Accordingly, their statistic is identical to that presented in [6] for passive source detection, demonstrating the equivalence of the two problems.

In this work, we derive a centralized GLRT detector that utilizes both Tx-Rx and Rx-Rx processing. The problem formulation explicitly accounts for the direct-path and target-path signals, noncoherent target scattering, and non-phase synchronized receivers. The resulting detector unifies both Tx-Rx and Rx-Rx processing in the PMR context, and enables comparison of the relative benefit provided by each type of processing to detection sensitivity. It is shown that Tx-Rx processing is more significant than Rx-Rx processing due to the signal-to-noise ratio (SNR) regimes typical of the direct-path and target-path signals in the PMR signal environment.

II. Signal Model

Consider a scenario with one target, N_t geographically distributed transmitters, and N_r geographically distributed array receivers. The target position and velocity are denoted by $\mathbf{p}$ and $\dot{\mathbf{p}}$, the transmitter positions (assumed known) by $\mathbf{t}^i$, $i = 1 \dots N_t$, and the receiver positions and velocities by $\mathbf{r}^j$ and $\dot{\mathbf{r}}^j$, $j = 1 \dots N_r$. Fig. 2 depicts the geometry and signal environment of the ij^{th} Tx-Rx pair.

As is typical in PMR, the direct-path and target-path signals are isolated in reference and surveillance channels via digital beamforming, shown in Fig. 2. Due to the large power ratio between the direct-path and target-path signals, which can exceed 100 dB, the surveillance channel is formed by steering in the target direction while nulling the transmitter direction. In practice, non-ideal nulling will necessitate further direct-path suppression via adaptive filtering [7]. The reference channel is formed by steering in transmitter direction, and any residual target-path leakage is insignificant due to its low power.

Following downconversion, anti-aliasing filtering, amplification, sampling, digital quadrature demodulation, decimation, and digital beamforming, the baseband reference and surveillance signals associated with the i^{th} transmitter at the j^{th} receiver are given by

$$\mathbf{s}_r^{ij} = \mu_r^{ij}\mathcal{D}_r^{ij}\mathbf{u}^i + \mathbf{n}_r^{ij} \quad (1)$$

$$\mathbf{s}_s^{ij} = \mu_s^{ij}\mathcal{D}_s^{ij}(\mathbf{p},\dot{\mathbf{p}})\,\mathbf{u}^i + \mathbf{n}_s^{ij}, \quad (2)$$

where $\mathbf{u}^i \in \mathbb{C}^{L\times 1}$ is the unit-norm $\left(\left\|\mathbf{u}^i\right\|^2 = 1\right)$ complex baseband signal emitted by the i^{th} transmitter with two-sided bandwidth B in Hertz and length $L = f_s T$, $f_s \geq B$ is the sampling rate, T is the coherent processing interval, $\mathcal{D}_r^{ij}$ and $\mathcal{D}_s^{ij}(\mathbf{p},\dot{\mathbf{p}})$ are the delay-Doppler operators that account for the delays and Doppler-shifts that result from propagation along the ij^{th} direct-path and target-path channels, respectively, $\mathbf{n}_r^{ij}$ and $\mathbf{n}_s^{ij}$ are independent complex baseband noise processes distributed as $\mathcal{CN}(\mathbf{0}_L, \sigma_r^2\mathbf{I}_L)$ and $\mathcal{CN}(\mathbf{0}_L, \sigma_s^2\mathbf{I}_L)$, respectively, and μ_r^{ij} and μ_s^{ij} are complex scale factors that account for the composite scaling of $\mathbf{u}^i$ associated with the ij^{th} direct-path and target-path channels. Note, the noise processes $\mathbf{n}_r^{ij}$ and $\mathbf{n}_s^{ij}$ are independent because the reference and surveillance channel steering vectors are orthogonal due to the transmitter null. Furthermore, $\sigma_r^2 = \sigma_s^2 \triangleq \sigma_n^2$ provided the steering vectors have equal norms, which is assumed here. Finally, the dependence of $\mathcal{D}_s^{ij}(\mathbf{p},\dot{\mathbf{p}})$ on $\mathbf{p}$ and $\dot{\mathbf{p}}$ is dropped in the sequel.

The complex scaling factors μ_r^{ij} and μ_s^{ij} are given by

$$\mu_r^{ij} = e^{j\left(\theta^j - \omega_c^i \tau^{ij}\right)} \sqrt{\frac{P_{\text{erp}}^i(\mathbf{r}^j)\lambda^{i2} G_{\text{rx}}^j(\mathbf{t}^i)}{(4\pi)^2 (R_0^{ij})^2}} \quad (3)$$

$$\mu_s^{ij} = \alpha^{ij} e^{j\left(\theta^j - \omega_c^i \tau^{ij}(\mathbf{p})\right)} \sqrt{\frac{P_{\text{erp}}^i(\mathbf{p})\lambda^{i2} G_{\text{rx}}^j(\mathbf{p})}{(4\pi)^3 (R_1^i R_2^j)^2}}, \quad (4)$$

where θ^j is a random phase associated with the j^{th} receiver, $\omega_c^i = 2\pi f_c^i$ is the transmitter carrier frequency, $P_{\text{erp}}^i(\mathbf{x})$ is the transmitter effective radiated power (ERP) in the direction of $\mathbf{x}$, $\lambda^i = c/f_c^i$ is the wavelength where c is the speed of light, $G_{\text{rx}}^j(\mathbf{x})$ is the receive antenna gain in the direction of $\mathbf{x}$, α^{ij} is the target's bistatic reflectivity as observed by the ij^{th} Tx-Rx pair, $R_0^{ij} = \left\|\mathbf{r}^j - \mathbf{t}^i\right\|$ is the direct-path propagation distance, $R_1^i = \left\|\mathbf{p} - \mathbf{t}^i\right\|$ and $R_2^j = \left\|\mathbf{r}^j - \mathbf{p}\right\|$ are the target-path propagation distances, $\tau^{ij} = R_0^{ij}/c$ is the direct-path delay, and $\tau^{ij}(\mathbf{p}) = (R_1^i + R_2^j)/c$ is the target-path delay.

III. Centralized GLRT Detector

We formulate the detection problem as a binary hypothesis test between alternative ($\mathcal{H}_1$) and null ($\mathcal{H}_0$) hypotheses,

$$\mathcal{H}_1: \quad \mathbf{s}_s^{ij} = \mu_s^{ij}\mathcal{D}_s^{ij}\mathbf{u}^i + \mathbf{n}_s^{ij} \quad (5)$$

$$\mathbf{s}_r^{ij} = \mu_r^{ij}\mathcal{D}_r^{ij}\mathbf{u}^i + \mathbf{n}_r^{ij} \quad (6)$$

$$\mathcal{H}_0: \quad \mathbf{s}_s^{ij} = \mathbf{n}_s^{ij} \quad (7)$$

$$\mathbf{s}_r^{ij} = \mu_r^{ij}\mathcal{D}_r^{ij}\mathbf{u}^i + \mathbf{n}_r^{ij}, \quad (8)$$

for $i = 1 \dots N_t$ and $j = 1 \dots N_r$. Note that $\mathcal{H}_1$ is a composite hypothesis, as the joint distribution of $\mathbf{s}_s^{ij}$ and $\mathbf{s}_r^{ij}$ is parameterized by the unknown target position $\mathbf{p}$ and velocity $\dot{\mathbf{p}}$, the scaling factors μ_r^{ij} and μ_s^{ij}, and the transmit signal $\mathbf{u}^i$, all of which are considered deterministic unknowns. Furthermore, $\mathcal{H}_0$ is also composite, parameterized by μ_r^{ij} and

$\mathbf{u}^i$. Accordingly, we derive the generalized likelihood ratio test (GLRT) detector. The GLRT detector is first derived using only the measurements associated with the i^{th} transmitter, after which the result is extended to all transmitters.

To begin, let $\mathbf{s}^i \in \mathbb{C}^{2N_r L \times 1}$ denote the vertical concatenation of all reference and surveillance channel measurements associated with the i^{th} transmitter, given by

$$\mathbf{s}^i = \left[\mathbf{s}_s^{i^T}\, \mathbf{s}_r^{i^T}\right]^T = \left[\mathbf{s}_s^{i1^T} \cdots \mathbf{s}_s^{iN_r^T}\, \mathbf{s}_r^{i1^T} \cdots \mathbf{s}_r^{iN_r^T}\right]^T. \quad (9)$$

Furthermore, let $\boldsymbol{\mu}^i \in \mathbb{C}^{2N_r \times 1}$ denote the vector of unknown scaling factors, given by

$$\boldsymbol{\mu}^i = \left[\boldsymbol{\mu}_s^{i^T}\, \boldsymbol{\mu}_r^{i^T}\right]^T = \left[\mu_s^{i1} \cdots \mu_s^{iN_r}\ \mu_r^{i1} \cdots \mu_r^{iN_r}\right]^T. \quad (10)$$

Then, due to the independence of all measurement noise processes, the log likelihood under $\mathcal{H}_1$ is

$$\ell(\mathbf{p}, \dot{\mathbf{p}}, \mathbf{u}^i, \boldsymbol{\mu}^i | \mathbf{s}^i; \mathcal{H}_1) = -\sum_{j=1}^{N_r} \left\|\mathbf{s}_r^{ij} - \mu_r^{ij} \mathcal{D}_r^{ij} \mathbf{u}^i\right\|^2 + \left\|\mathbf{s}_s^{ij} - \mu_s^{ij} \mathcal{D}_s^{ij} \mathbf{u}^i\right\|^2. \quad (11)$$

It can be shown that the maximum likelihood estimate of $\mu_{(r,s)}^{ij}$, conditioned on the remaining unknowns, is given by

$$\hat{\mu}_{(r,s)}^{ij} = \left(\mathcal{D}_{(r,s)}^{ij} \mathbf{u}^i\right)^H \mathbf{s}_{(r,s)}^{ij}. \quad (12)$$

Substituting (12) into (11), and simplifying,

$$\ell(\mathbf{p}, \dot{\mathbf{p}}, \mathbf{u}^i, \hat{\boldsymbol{\mu}}^i | \mathbf{s}^i; \mathcal{H}_1) = -\left\|\mathbf{s}^i\right\|^2 + \mathbf{u}^{i^H} \Phi_1^i \Phi_1^{i^H} \mathbf{u}^i, \quad (13)$$

where $\Phi_1^i = [\Phi_s^i\ \Phi_r^i] \in \mathbb{C}^{L \times 2N_r}$, $\Phi_s^i = [\tilde{\mathbf{s}}_s^{i1} \cdots \tilde{\mathbf{s}}_s^{iN_r}] \in \mathbb{C}^{L \times N_r}$, $\Phi_r^i = [\tilde{\mathbf{s}}_r^{i1} \cdots \tilde{\mathbf{s}}_r^{iN_r}] \in \mathbb{C}^{L \times N_r}$, and $\tilde{\mathbf{s}}_s^{ij} = (\mathcal{D}_s^{ij})^H \mathbf{s}_s^{ij}$ and $\tilde{\mathbf{s}}_r^{ij} = (\mathcal{D}_r^{ij})^H \mathbf{s}_r^{ij}$ represent delay- and Doppler-compensated reference and surveillance channel signals, respectively.

The quadratic form in (13) is maximized when $\mathbf{u}^i$ equals the eigenvector associated with the largest eigenvalue of $\Phi_1^i \Phi_1^{i^H}$. Inserting this maximum likelihood estimate of $\mathbf{u}^i$ into (13),

$$\ell(\mathbf{p}, \dot{\mathbf{p}}, \hat{\mathbf{u}}^i, \hat{\boldsymbol{\mu}}^i | \mathbf{s}^i; \mathcal{H}_1) = -\left\|\mathbf{s}^i\right\|^2 + \lambda_{\max}\left(\Phi_1^i \Phi_1^{i^H}\right), \quad (14)$$

where $\lambda_{\max}(\mathbf{M})$ denotes the largest eigenvalue of $\mathbf{M}$. Since the eigenvalues of $\Phi_1^i \Phi_1^{i^H} \in \mathbb{C}^{L \times L}$ and $\Phi_1^{i^H} \Phi_1^i \in \mathbb{C}^{2N_r \times 2N_r}$ are equal, and typically $2N_r \ll L$, it is more efficient to instead consider $\mathbf{G}_1^i = \Phi_1^{i^H} \Phi_1^i$, the *Gram matrix*, giving

$$\ell(\mathbf{p}, \dot{\mathbf{p}}, \hat{\mathbf{u}}^i, \hat{\boldsymbol{\mu}}^i | \mathbf{s}^i; \mathcal{H}_1) = -\left\|\mathbf{s}^i\right\|^2 + \lambda_{\max}\left(\mathbf{G}_1^i\right). \quad (15)$$

Note that $\mathbf{G}_1^i(\mathbf{p}, \dot{\mathbf{p}})$ can be partitioned into four blocks,

$$\mathbf{G}_1^i(\mathbf{p}, \dot{\mathbf{p}}) = \begin{bmatrix} \Phi_s^{i^H}(\mathbf{p}, \dot{\mathbf{p}}) \\ \Phi_r^{i^H} \end{bmatrix} \left[\Phi_s^i(\mathbf{p}, \dot{\mathbf{p}})\ \Phi_r^i\right] \quad (16)$$

$$\triangleq \begin{bmatrix} \mathbf{G}_{ss}^i(\mathbf{p}, \dot{\mathbf{p}}) & \mathbf{G}_{sr}^i(\mathbf{p}, \dot{\mathbf{p}}) \\ \mathbf{G}_{rs}^i(\mathbf{p}, \dot{\mathbf{p}}) & \mathbf{G}_{rr}^i \end{bmatrix}, \quad (17)$$

where $\left(\mathbf{G}_{rs}^i(\mathbf{p}, \dot{\mathbf{p}})\right)^H = \mathbf{G}_{sr}^i(\mathbf{p}, \dot{\mathbf{p}})$. Each block is itself a Gram matrix consisting of the inner products of (a) the set of reference or surveillance signals with (b) the set of reference or surveillance signals, discussed further in Sec. IV.

By a similar procedure, it can be shown that the log-likelihood under $\mathcal{H}_0$ is given by

$$\ell(\hat{\mathbf{u}}^i, \hat{\boldsymbol{\mu}}_r^i | \mathbf{s}^i; \mathcal{H}_0) = -\left\|\mathbf{s}^i\right\|^2 + \lambda_{\max}\left(\mathbf{G}_0^i\right), \quad (18)$$

where $\mathbf{G}_0^i = \Phi_r^{i^H} \Phi_r^i$.

Using (15) and (18), the GLRT that considers only the measurements associated with the i^{th} transmitter is given by

$$\max_{\tilde{\mathbf{p}}, \tilde{\dot{\mathbf{p}}}} \left\{\lambda_{\max}\left(\mathbf{G}_1^i(\tilde{\mathbf{p}}, \tilde{\dot{\mathbf{p}}})\right)\right\} - \lambda_{\max}(\mathbf{G}_0^i) \underset{\mathcal{H}_0}{\overset{\mathcal{H}_1}{\gtrless}} \kappa^i, \quad (19)$$

where $\tilde{\mathbf{p}}$ and $\tilde{\dot{\mathbf{p}}}$ denote hypothesized target position and velocity, respectively. Due to the independence of the receiver noise between channels, the GLRT that considers all measurements follows immediately, given by

$$\max_{\tilde{\mathbf{p}}, \tilde{\dot{\mathbf{p}}}} \left\{\sum_{i=1}^{N_t} \lambda_{\max}\left(\mathbf{G}_1^i(\tilde{\mathbf{p}}, \tilde{\dot{\mathbf{p}}})\right)\right\} - \sum_{i=0}^{N_t} \lambda_{\max}\left(\mathbf{G}_0^i\right) \underset{\mathcal{H}_0}{\overset{\mathcal{H}_1}{\gtrless}} \kappa. \quad (20)$$

In the following, (20) is compared to the detector that results when the problem formulation considers only target-path signals, given by

$$\max_{\tilde{\mathbf{p}}, \tilde{\dot{\mathbf{p}}}} \left\{\sum_{i=1}^{N_t} \lambda_{\max}\left(\mathbf{G}_{ss}^i(\tilde{\mathbf{p}}, \tilde{\dot{\mathbf{p}}})\right)\right\} \underset{\mathcal{H}_0}{\overset{\mathcal{H}_1}{\gtrless}} \nu. \quad (21)$$

Note that (21), termed the *Rx-Rx detector*, is the result of [4] extended to multiple transmitters, assuming the target-path signals are isolated via beamforming as described in Sec. II.

IV. Analysis

Insight is provided by examining the structure of the Gram matrices in (17). First, the elements of $\mathbf{G}_{ss}^i(\tilde{\mathbf{p}}, \tilde{\dot{\mathbf{p}}})$ consist of the pairwise inner products of delay-Doppler compensated surveillance channels, where the delay-Doppler compensation is referenced to $(\tilde{\mathbf{p}}, \tilde{\dot{\mathbf{p}}})$. This represents Rx-Rx processing, which localizes a target along curves of constant TDOA (range difference) and FDOA (range difference rate). Similarly, the elements of $\mathbf{G}_{sr}^i(\tilde{\mathbf{p}}, \tilde{\dot{\mathbf{p}}})$ consist of the pairwise inner products of delay-Doppler compensated surveillance channels with delay-Doppler compensated reference channels, where the surveillance channels are compensated according to $(\tilde{\mathbf{p}}, \tilde{\dot{\mathbf{p}}})$ and the reference channels according to $\mathbf{t}^i$. This represents Tx-Rx processing, which localizes a target along curves of constant bistatic range and bistatic range rate.

This interpretation is confirmed by numerical example in Fig. 3, which depicts $\lambda_{\max}\left(\mathbf{G}_{ss}^i(\tilde{\mathbf{p}}, \tilde{\dot{\mathbf{p}}})\right)$ and $\lambda_{\max}\left(\mathbf{G}_{sr}^i(\tilde{\mathbf{p}}, \tilde{\dot{\mathbf{p}}})\right)$ as a function of $\tilde{\mathbf{p}}$ for a scenario consisting of one transmitter, three receivers, and one target, all stationary. This scenario is described fully in Sec. V. As expected, the response in the vicinity of the target is oriented along target-referenced iso-range difference hyperbolas in Fig. 3a, and along iso-bistatic range ellipses in Fig. 3b. Furthermore, $\lambda_{\max}\left(\mathbf{G}_{sr}^i(\tilde{\mathbf{p}}, \tilde{\dot{\mathbf{p}}})\right)$ exceeds $\lambda_{\max}\left(\mathbf{G}_{ss}^i(\tilde{\mathbf{p}}, \tilde{\dot{\mathbf{p}}})\right)$ by 38.8 dB at $\tilde{\mathbf{p}} = \mathbf{p}$. This is explained in terms of the power difference between the direct-path and target-path signals. Specifically, noting that $\lambda_{\max}\left(\mathbf{G}_{ss}^i(\tilde{\mathbf{p}}, \tilde{\dot{\mathbf{p}}})\right) = \lambda_{\max}\left(\Phi_s^i \Phi_s^{i^H}\right)$, it can be seen by inspection that the largest eigenvalue in the noiseless

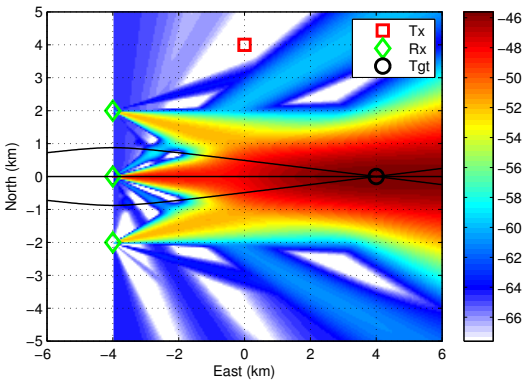

(a) $\lambda_{\max}\left(\mathbf{G}^i_{ss}(\tilde{\mathbf{p}},\dot{\tilde{\mathbf{p}}})\right)\Big|_{\dot{\tilde{\mathbf{p}}}=0}$ (dB)

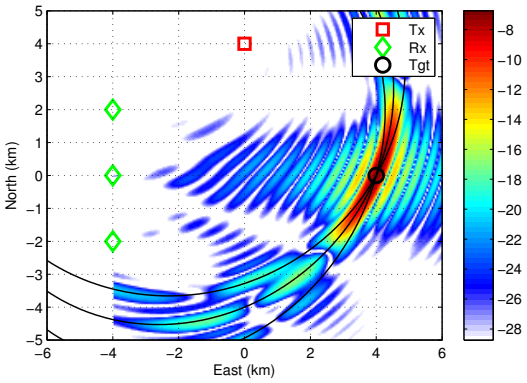

(b) $\lambda_{\max}\left(\mathbf{G}^i_{sr}(\tilde{\mathbf{p}},\dot{\tilde{\mathbf{p}}})\right)\Big|_{\dot{\tilde{\mathbf{p}}}=0}$ (dB)

Fig. 3. Demonstration of (a) Rx-Rx and (b) Tx-Rx processing. Target-referenced contours of iso-range difference and iso-bistatic range are depicted as solid black lines in (a) and (b), respectively.

case equals $\boldsymbol{\mu}_s^{i\,H}\boldsymbol{\mu}_s^i = \left\|\boldsymbol{\mu}_s^i\right\|^2$, since Φ_s^i is rank 1 at the true target location. Similarly, $\lambda_{\max}\left(\mathbf{G}^i_{sr}(\mathbf{p},\dot{\mathbf{p}})\right) = \boldsymbol{\mu}_r^{i\,H}\boldsymbol{\mu}_s^i$. Defining $\rho^{ij}(\mathbf{p}) = |\mu_r^{ij}|^2/|\mu_s^{ij}(\mathbf{p})|^2$ as the power ratio between the reference and surveillance channels, then

$$\boldsymbol{\mu}_r^{i\,H}\boldsymbol{\mu}_s^i = \sum_{j=1}^{N_r}\sqrt{\rho^{ij}(\mathbf{p})}\,|\mu_s^{ij}(\mathbf{p})|^2 \geq \sqrt{\rho^i_{\min}(\mathbf{p})}\,\left\|\boldsymbol{\mu}_s^i\right\|^2, \quad (22)$$

where $\rho^i_{\min}(\mathbf{p})$ is the minimum power ratio over all receivers. Consequently, $\boldsymbol{\mu}_r^{i\,H}\boldsymbol{\mu}_s^i/\left\|\boldsymbol{\mu}_s^i\right\|^2 \geq \sqrt{\rho^i_{\min}(\mathbf{p})}$. In this example, the minimum power ratio is $\rho^i_{\min}(\mathbf{p}) = 74.98$ dB, giving $\boldsymbol{\mu}_r^{i\,H}\boldsymbol{\mu}_s^i/\left\|\boldsymbol{\mu}_s^i\right\|^2 \geq 37.49$ dB, which is consistent with Fig. 3.

This suggests that the contribution of Rx-Rx processing to the test statistic (20) might be insignificant in comparison to Tx-Rx processing due to the large power ratio between direct-path and target-path signals. For instance, Fig. 4 depicts the power ratio as a function of target position for a 10 dBsm target as observed by one receiver in the preceding example. As shown, the power ratio ranges between 60 and 90 dB over most of the surveillance region, which is typical of the passive radar signal environment [8].

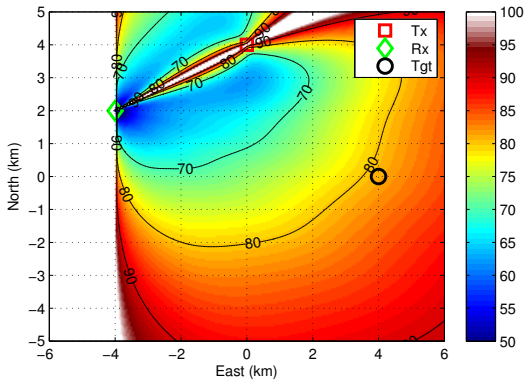

Fig. 4. Power ratio $\rho^{ij}(\mathbf{p})$ (dB) as a function of target location $\mathbf{p}$ for a 10 dBsm target.

V. Numerical Example

A numerical example is presented to demonstrate the performance of the derived detector. The scenario consists of two stationary transmitters at $\mathbf{t}^1 = [0, -4]$ km and $\mathbf{t}^2 = [0, 4]$ km, three stationary receivers at $\mathbf{r}^1 = [-4, 0]$ km, $\mathbf{r}^2 = [-4, 2]$ km, and $\mathbf{r}^3 = [-4, -2]$ km, and a single stationary target at $\mathbf{p} = [4, 0]$ km. A stationary scenario is chosen to clearly illustrate the spatial structure of the test statistic, although the formulation encompasses moving platforms and can exploit Doppler for localization. The transmitters emit signals with 500 kHz bandwidth, carrier frequencies of 400 MHz and 410 MHz, respectively, and isotropic 50 W ERP. All receivers consist of East-facing 6-element ULAs with approximately $\lambda/2$ element spacing and $\cos(\theta_{az})$ element patterns. Complex baseband surveillance and reference signals are simulated according to the signal model of Sec. II with f_s = 500 kHz and T = 20 ms. The receivers are not phase-synchronized due to the random phase θ_j in (3) and (4). The noise processes are scaled to match the expected SNRs following beamforming for receivers that have 6 dB noise figures and 20 MHz RF front-end bandwidths, sample at 40 MHz using ideal 12 bit ADCs, perform digital quadrature demodulation, and decimate each channel to a 500 kHz sampling rate. The target is simulated with an isotropic 10 dBsm RCS, although a spatially-fluctuating RCS is also accommodated. In this example, the average target-path SNR is -31.0 dB per receiver element and -7.24 dB following decimation and beamforming. The corresponding direct-path SNRs are 47.48 and 71.28 dB, respectively, giving an average power ratio of about 78.5 dB.

Fig. 5a depicts the GLRT test statistic (20) as a function of hypothesized position $\tilde{\mathbf{p}}$. Note that the dominant responses are aligned with the Tx-Rx pair bistatic ellipses, with no discernible response along the Rx-Rx pair hyperbolas, confirming that Tx-Rx processing influences the test statistic more significantly than Rx-Rx processing. Fig. 5b depicts the test statistic that results from the Rx-Rx detector statistic (21), which performs Rx-Rx processing on the target-path signals alone. In contrast to the noiseless case shown previously in Fig. 3a, in which a peak is apparent at the target location, the

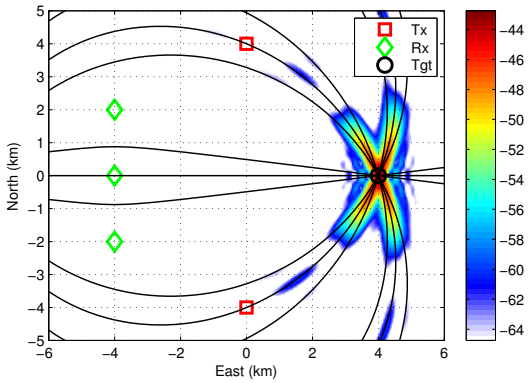

(a) $\sum_{i=0}^{N_t} \lambda_{\max}\left(\mathbf{G}_1^i(\tilde{\mathbf{p}},\tilde{\mathbf{p}})\right)\Big|_{\tilde{\mathbf{p}}=0} - \sum_{i=0}^{N_t} \lambda_{\max}\left(\mathbf{G}_0^i\right)$ (dB)

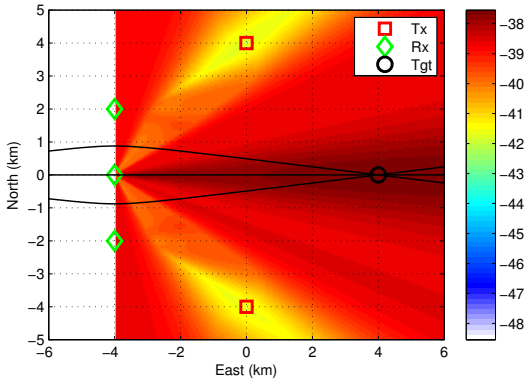

(b) $\sum_{i=0}^{N_t} \lambda_{\max}\left(\mathbf{G}_{ss}^i(\tilde{\mathbf{p}},\tilde{\mathbf{p}})\right)\Big|_{\tilde{\mathbf{p}}=0}$ (dB)

Fig. 5. Spatial distribution of the test statistics of (a) the GLRT detector and (b) Rx-Rx processing detector.

test statistic in Fig. 5b is significantly more dispersed with a 3 dB depression around each transmitter that results from transmitter nulling during surveillance channel formation[2]. This indicates that noise significantly degrades the target response, which is not unexpected due to the negative target-path SNRs in this scenario.

Detection performance is investigated numerically by calculating receiver operating characteristic (ROC) curves over a range of target SNRs for both the GLRT detector (20) and the Rx-Rx detector (21), shown in Fig. 6. Consistent with the convention in radar, the target SNR is expressed in terms of the SNR that would result following ideal matched filtering, even though such processing is not performed here. Thus, the SNRs here include an additional 40 dB signal processing gain. For example, -7.24 dB SNR following beamforming is equivalent to 32.76 dB SNR on this scale. In comparison, the GLRT detector realizes comparable performance at target SNRs approximately 20 dB lower than the Rx-Rx detector.

[2]Figs. 3a and 5b show 22 dB and 11 dB of dynamic range, respectively.

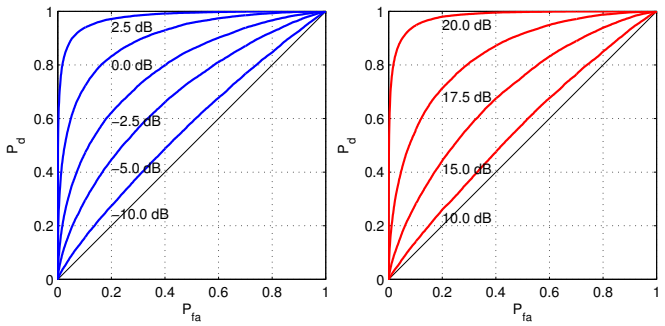

(a) (b)

Fig. 6. ROC curves for (a) the GLRT detector and (b) Rx-Rx detector.

VI. Conclusion

Although the PMR signal environment supports source localization techniques, it appears such techniques are of limited utility for the PMR problem due to the SNR regimes typical of the PMR signal environment. In particular, the large power ratio between the direct-path and target-path signals renders Rx-Rx processing techniques that exploit only the target-path signals insignificant in comparison to Tx-Rx processing techniques that exploit both the direct-path and target-path signals. We have reached this conclusion by deriving a GLRT detector that exploits both types of processing, showing that Tx-Rx processing has the dominant effect on the resulting test statistic, and demonstrating that this detector is superior to the Rx-Rx detector in detection sensitivity.

References

[1] M. Malanowski and K. Kulpa, "Optimization of confirmation time of bistatic tracks in passive radar," *IEEE Trans. Aerosp. Electron. Syst.*, vol. 47, no. 2, pp. 1060–1072, 2011.

[2] D. Hack, L. Patton, A. Kerrick, and M. Saville, "Direct Cartesian detection, localization, and de-ghosting for passive multistatic radar," in *Proc. IEEE Sensor Array and Multichannel Signal Processing Workshop (SAM)*, 2012.

[3] L. Wang and B. Yazici, "Passive imaging of moving targets with sparsely distributed receivers," in *Proc. IEEE Radar Conf. (RADAR)*, 2011, pp. 073–078.

[4] K. S. Bialkowski, I. V. L. Clarkson, and S. D. Howard, "Generalized canonical correlation for passive multistatic radar detection," in *Proc. IEEE Statistical Signal Processing Workshop (SSP)*, 2011, pp. 417–420.

[5] M. Skolnik, *Introduction to Radar Systems*. New York, NY: McGraw-Hill, 2001.

[6] N. Vankayalapati and S. Kay, "Asymptotically optimal detection of low probability of intercept signals using distributed sensors," *IEEE Trans. Aerosp. Electron. Syst.*, vol. 48, no. 1, pp. 737–748, 2012.

[7] F. Colone, D. W. O'Hagan, P. Lombardo, and C. J. Baker, "A multistage processing algorithm for disturbance removal and target detection in passive bistatic radar," *IEEE Trans. Aerosp. Electron. Syst.*, vol. 45, no. 2, pp. 698–722, 2009.

[8] D. Gould, R. Pollard, C. Sarno, and P. Tittensor, "Developments to a multiband passive radar demonstrator system," in *Proc. IET Int Radar Systems Conf*, 2007, pp. 1–5.